Numerical simulation of an elastoplastic plate via mixed finite elements

LUCIA DELLA CROCE[1], PAOLO VENINI[2] and ROBERTO NASCIMBENE[2]
[1]*Department of Mathematics, University of Pavia, Via Ferrata 1, 27100 Pavia, Italy*
(E-mail: luciadc@dimat.unipv.it)
[2]*Department of Structural Mechanics, University of Pavia, Via Ferrata 1, 27100, 11 Pavia, Italy*
(E-mails: paolo.venin@unipv.it, roberto.nascimbene@unipv.it)

Abstract. A mixed interpolated formulation for the analysis of elastoplastic Reissner-Mindlin plates is presented. Special attention is given to the limit case of very small thickness that is well known to lead to inaccurate numerical solutions, unless ad-hoc remedies are taken into account to avoid locking (such as reduced or selective integration schemes). The finite element presented herein combines the higher-order approach with the mixed-interpolated formulation of linear elastic problems. This mixed element has been herein extended to the elasto-plastic behavior, using a J_2 approach with yield function depending on moments and shear stresses. A backward-Euler procedure is then used to map the elastic trial stresses back to the yield surface with the aid of a Newton-Raphson approach to solve the nonlinear system and without the calculation of the consistent tangent matrix. The element is shown to be very effective for the class of benchmark problems analyzed and does not present any locking or instability tendencies, as illustrated by various representative examples.

Key words: elasto-plastic analysis, mixed finite element, Reissner-Mindlin plate

1. Introduction

A tremendous effort has been recently put in the development of numerical methods for the analysis of nonlinear solids and materials. New concepts such as multiscale analysis [1], fractals [2], localization [3, 4], size effects [5, 6] and multifield theories [7, 8], just to mention a few, have been investigated giving rise to entirely new branches of the mechanics of solids. Textbooks that are nowadays classical, such as [9–13], deal with several aspects of material nonlinearity, focussing in particular on continuum plasticity even at large strains.

Conversely, considerably less attention has been paid to nonlinear material behavior at the structural level. Although a wide range of works concerning linear elastic plates are available in the scientific literature [14–17], on the contrary not many contributions are available in the recent literature concerning the analysis of elastoplastic Reissner-Mindlin plates at the thin limit that are herein dealt with [18, 19]. Among them, a pioneering contribution seems to be [20] that has developed a shell element whose behavior in the inelastic limit plate case resembles closely the well-known four-noded element by Bathe and Dvorkin [21]. Further contributions come from [22, 23] that have put forth a step-marching methodology for thick elastoplastic plates whereby stress updates and consistency are imposed simultaneously via a linearized coupled system of equations. Attention is paid in [23] to the definition of a consistent tangent matrix that is crucial in order to preserve the expected convergence order [10]. In [24] a four-node element with assumed shear strains and incompatible bending modes is

introduced that operates on stress resultant and allows separate calculations for consistency parameter and stress updates. More recently, see [25], a direct domain/boundary-element method has been proposed for the inelastic dynamic analysis of Reissner-Mindlin plates.

For completeness' sake, we should, however, mention that Reissner-Mindlin plates in the elastic regime have been enjoying continuous interest and appealing locking-free strategies for their numerical simulation are still being proposed, see [26–29] among others, mostly within the framework of the finite-element method [30].

In the present work, a *novel* approach to the analysis of elastoplastic Reissner-Mindlin plates is presented. Here *novel* means that a finite-element mixed interpolated approach in elasticity field, has been combined with a plastic corrector algorithm to solve the nonlinear material problem. As to the discretization, the method is an extension of the hierarchical one extensively tested in the linear elastic case in the recent past, [31–35].

Serendipity and bubble elements are successfully adopted in order to get a stable and convergent approximation with an exact thin limit. Elastoplasticity is dealt with in a rather non-standard manner by means of an elastic-predictor plastic-corrector approach in which consistency parameters and stress updates are simultaneously evaluated [23] without using a consistent tangent operator as usual done in classical plasticity approach [9].

The layout of the paper is as follows. In Section 2 we briefly recall the variational form governing the behavior of elastic Reissner-Mindlin form along with its continuous elastoplastic extension. We make use of a standard J_2 hardening idealization and arrive at an explicit expression for the tangent stiffness matrix. In Section 3 the discrete variational problem is set forth followed by a detailed presentation of our predictor-corrector algorithm. Section 4 presents the outcomes of a few numerical tests that give further substance to the theoretical model, also through convincing comparisons with the (few) shear existing results in the literature, [23, 24]. Conclusions and need for future work are left to Section 5.

2.   Continuous problem

This section deals with the continuous Reissner-Mindlin problem and is conceptually divided into two main parts. In the first one, see Section 2.1, we briefly recall the equations governing the elastic Reissner-Mindlin plate in variational form. The elastic variational equations are of the utmost importance in view of the extension to the elastoplastic case that may in fact be framed as a variational inequality [38, 39]. The second part, see Sections 2.2 and 2.3, presents the extension to elastoplasticity through the introduction of the adopted Mises yielding function and the plasticity constitutive law in incremental form [9, 12, 17].

2.1.   Elastic Reissner-Mindlin plate equations

We start by presenting the linear theory used to describe the elastic behavior of the plate within the framework set forth by Reissner and Mindlin ([18, 19]). The theory takes into account transverse shear deformations and uses the assumption that particles of the plate originally on a line that is normal to the undeformed middle surface remain on a straight line during deformation, but this line is not necessarily normal to the deformed middle surface. Furthermore, the so-called in-plane displacements u and v and the normal displacement w are given the following standard form

$$u(x, y, z) = z\theta_x(x, y), \quad v(x, y, z) = z\theta_y(x, y), \quad w(x, y, z) = w(x, y). \tag{1}$$

The functions θ_x and θ_y are the rotations of the normal to the undeformed middle surface in the $x - z$ and $y - z$ planes, respectively. The three components of curvature vector χ and the vector of the transverse shear γ are defined as

$$\chi = \begin{bmatrix} \theta_{x,x} \\ \theta_{y,y} \\ \theta_{x,y} + \theta_{y,x} \end{bmatrix}, \quad \gamma = \begin{bmatrix} w,_x + \theta_x \\ w,_y + \theta_y \end{bmatrix}. \tag{2}$$

Curvatures χ and shear strains γ are usually collected in a generalized strain vector $\mathbf{E}$ as

$$\mathbf{E} = \begin{bmatrix} \chi \\ \gamma \end{bmatrix}. \tag{3}$$

Stress components of the plate may be grouped in the generalized resultant stress vector Σ that reads

$$\Sigma = [M_x \ M_y \ M_{xy} \ Q_x \ Q_y]^T, \tag{4}$$

where we may of course distinguish between moments $[M_x, M_y, M_{xy}]^T$ and transverse shears $[Q_x, Q_y]^T$. Under the hypothesis of linear elasticity and isotropic behavior, the constitutive law may be written as

$$\Sigma = \mathbf{D}^e \mathbf{E}, \ \mathbf{D}^e = \begin{bmatrix} \mathbf{D}_b & 0 \\ 0 & \mathbf{D}_s \end{bmatrix}, \tag{5}$$

where $\mathbf{D}^e$ is the elastic Reissner-Mindlin matrix. In Equation (5), $\mathbf{D}_b$ and $\mathbf{D}_s$ are the moment/curvature and shear-stress/rotation constitutive matrices that may be written as

$$\mathbf{D}_b = \frac{Et^3}{12(1 - \nu^2)} \begin{bmatrix} 1 & \nu & 0 \\ \nu & 1 & 0 \\ 0 & 0 & \frac{1 - \nu}{2} \end{bmatrix}, \quad \mathbf{D}_s = \frac{Etk}{2(1 + \nu)} \begin{bmatrix} 1 & 0 \\ 0 & 1 \end{bmatrix}. \tag{6}$$

The constant E is the Young's modulus, ν the Poisson's ratio, t the thickness of the plate and k the shear-correction factor, that is the ratio between the actual cross sectional area and an ideal one corresponding to an hypothetical uniform shear distribution; k depends on the plate properties and is often set equal to $\frac{5}{6}$ for isotropic homogeneous plates. The strain energy is additively decomposed into the bending and shear contributions and can be written as $U = \mathcal{U}_b + \mathcal{U}_s$ where

$$\mathcal{U}_b = \frac{1}{2} \int_\Omega \chi^T \mathbf{D}_b \chi \, \mathrm{d}\Omega, \text{ and } \mathcal{U}_s = \frac{1}{2} \int_\Omega \gamma^T \mathbf{D}_s \gamma \, \mathrm{d}\Omega, \tag{7}$$

where Ω denotes the undeformed middle surface of the plate and Γ his boundary. The stationarity of the potential energy allows one to write

$$\int_\Omega \delta\chi^T \mathbf{D}_b \chi \, \mathrm{d}\Omega + \int_\Omega \delta\gamma^T \mathbf{D}_s \gamma \, \mathrm{d}\Omega - \int_\Omega \delta w q \, \mathrm{d}\Omega = 0, \tag{8}$$

which is basically the principle of virtual displacements for the plate. Let us introduce the following functional spaces:

– $H_0^1(\Omega)$ the space of distributions which together with their first derivatives are in $L^2(\Omega)$, and whose traces on Γ vanish:

$$H_0^1(\Omega) = \left\{ w | w \in L^2(\Omega) : \left(\frac{\partial w}{\partial x}, \frac{\partial w}{\partial y} \right) \in L^2(\Omega), w | \Gamma = 0 \right\}, \tag{9}$$

– $L^2(\Omega)$ the space of square integrable functions in Ω:

$$L^2(\Omega) = \left\{ w | \int_\Omega |w|^2 \mathrm{d}x = ||w||^2_{L^2(\Omega)} < +\infty \right\}. \tag{10}$$

Both $H_0^1(\Omega)$ and $L^2(\Omega)$ are Hilbert spaces endowed with the classical inner products [40]. Using the previous definitions, we frame Equation (8) in proper functional spaces arriving at the following variational formulation

$$\begin{cases} \text{Find } (\vec{\theta}, w) \in (H_0^1)^2 \times H_0^1 \text{ such that} \\ \\ \dfrac{E}{12(1 - v^2)} \mathcal{A}(\vec{\theta}, \vec{\psi}) + \dfrac{E t^{-2} k}{(1 + v)} ||\nabla w - \vec{\theta}||^2_0 = (q, v) \\ \\ \forall (\vec{\psi}, v) \in (H_0^1)^2 \times H_0^1, \end{cases} \tag{11}$$

where $\vec{\theta} = (\theta_x, \theta_y)$ and $\mathcal{A}(\vec{\theta}, \vec{\psi})$ is the bilinear form

$$\begin{aligned} \mathcal{A}(\vec{\theta}, \vec{\psi}) = \int_\Omega & \left[\theta_{x,x} \psi_{x/x} + \theta_{y,y} \psi_{y/y} + v(\theta_{x,x} \psi_{y/y} + \theta_{y,y} \psi_{x/x}) \right. \\ & \left. + \frac{1 - v}{2} (\theta_{x,y} + \theta_{y,x})(\psi_{x/y} + \psi_{y/x}) \right] \mathrm{d}\Omega. \end{aligned} \tag{12}$$

2.2. THE VON MISES YIELD CRITERION

The yield criterion determines the stress level at which plastic deformations occur and can be written in the general form

$$f(\Sigma, H) = 0, \tag{13}$$

where H is the hardening modulus. The yield condition can be interpreted as a convex surface in the n-dimensional stress space whose center moves according to the evolution of the so-called backstress. Notice, however, that no hardening will be considered in the subsequent analytical formulation as well as within the numerical investigations to be presented and discussed next. Different classes of material exhibit different elasto-plastic characteristic. For metals for instance experimental observations indicate that the plastic deformation is independent of the pressure. By looking at the bending deformation only, the classical plane-stress version of the Von Mises yield function is:

$$f = (M_x^2 + M_y^2 + 3M_{xy}^2)^{1/2} - M_0, \tag{14}$$

where M_0 is the equivalent yield moment. In the case of shear deformable plates, the Von Mises plasticity condition can be generalized and formulated in term of the stress resultants. The idea of using a stress resultant yield function is justified by a good approximation of thin plates and can be recovered from the works of Shapiro and Ivanov ([41, 42]). More recent developments are employed in the works of Ibrahimbegovic [24] and Papadopoulos-Taylor [22], where the Von Mises criterion assumes the following general quadratic form

$$f(\Sigma) = \Sigma^T A \Sigma - 1 = \frac{16}{\sigma_0^2 t^4} \left[M_x^2 + M_y^2 - M_x M_y + 3M_{xy}^2 \right] + \frac{3}{t^2 \sigma_0^2} \left[Q_x^2 + Q_y^2 \right] - 1, \quad (15)$$

where σ_0 is the uniaxial yielding stress. From Equation (15), the following choice was made in our computations for matrix A:

$$A = \frac{1}{\sigma_0^2 t^2} \begin{bmatrix} \dfrac{16}{t^2} & -\dfrac{8}{t^2} & 0 & 0 & 0 \\[2mm] -\dfrac{8}{t^2} & \dfrac{16}{t^2} & 0 & 0 & 0 \\[2mm] 0 & 0 & \dfrac{48}{t^2} & 0 & 0 \\[2mm] 0 & 0 & 0 & 3 & 0 \\[2mm] 0 & 0 & 0 & 0 & 3 \end{bmatrix}. \quad (16)$$

Adopting a more compact form, we then can write the yield function as:

$$f = ||\Sigma||_A^2 - 1, \quad (17)$$

where

$$||\Sigma||_A = |\Sigma^T A \Sigma|^{1/2}. \quad (18)$$

For completeness' sake, one should note that isotropic and kinematic hardening could easily be incorporated within the adopted framework.

2.3. CONSTITUTIVE ELASTIC-PLASTIC LAW

In this section the essential features of the elastoplastic behavior are recalled and the basic expressions are described in a form suitable for numerical approximation. We recall here the essential form of vector, matrix and tensor equations governing the stress state in the case of elastoplastic response assuming a small deformation regime, referring to [9, 12] for more details. Due to an infinitesimal stress increment, strain increments are additively decomposed into an elastic and a plastic part:

$$d\mathbf{E} = d\mathbf{E}^e + d\mathbf{E}^p. \quad (19)$$

Following previous notations, in the case of Reissner-Mindlin plates we may then write

$$d\mathbf{E} = \begin{bmatrix} d\chi^e \\ d\gamma^e \end{bmatrix} + \begin{bmatrix} d\chi^p \\ d\gamma^p \end{bmatrix}. \quad (20)$$

The elastic component $d\mathbf{E}^e$ depends linearly on the elastic stress and may be written according to the standard rule

$$d\mathbf{E}^e = (\mathbf{D}^e)^{-1} d\Sigma. \quad (21)$$

As to the plastic-strain increment $d\mathbf{E}^p$, we shall adopt the classical relation of associative plasticity that reads

$$dE^p = d\lambda \frac{\partial f}{\partial \Sigma} = d\lambda \mathbf{a}, \tag{22}$$

where $d\lambda$ is a positive constant usually referred to as the *plastic-strain-rate multiplier* and vector $\mathbf{a}$ is normal to the yield surface. In the case of Mises plasticity, direct differentiation of Equation (15) allows one to write

$$\mathbf{a} = 2\mathbf{A}\Sigma. \tag{23}$$

During a *pseudo-time* increment, stress and strain updates are therefore related by the relation

$$d\Sigma = D(dE^t - dE^p) = D(dE^t - d\lambda \mathbf{a}), \tag{24}$$

where a superposed t means total (strain) increment. For plastic flow to occur, the further condition of persistency of the stress onto the yield surface must be fulfilled. One may therefore write

$$\mathbf{a}^T d\Sigma = 0, \tag{25}$$

i.e., the stress change $d\Sigma$ is instantaneously tangent to the yield surface. In order to obtain a complete elastoplastic incremental stress-strain relation of the type

$$d\Sigma = \mathbf{D}^{ep} dE, \tag{26}$$

i.e., to compute the tangent stiffness matrix, Equation (24) is pre-multiplied by the vector $\mathbf{a}^T$ and, using Equation (25), the plastic strain multiplier can be written as

$$d\lambda = \frac{\mathbf{a}^T \mathbf{D} dE}{\mathbf{a}^T \mathbf{D} \mathbf{a}}. \tag{27}$$

Substituting (27) in (24), one obtains the tangent elastoplastic stiffness matrix as

$$\mathbf{D}^{ep} = \mathbf{D} \left(\mathbf{I} - \frac{\mathbf{a}\mathbf{a}^T \mathbf{D}}{\mathbf{a}^T \mathbf{D} \mathbf{a}} \right). \tag{28}$$

3. Discrete approximation

The numerical solution of the elasto-plastic problem is performed in two main substeps that are dealt with in much detail in the two following sections. One has first to solve the elastic trial problem and then, when the relevant stress state does not belong to the current elastic domain, a procedure to solve nonlinear systems is needed for mapping the stress back to the yielding surface. As to the first step, we use a mixed-interpolated formulation of the Reissner-Mindlin plate problem. The second step is handled via a modified Newton-Raphson approach that does not need the usual recalculation of the tangent stiffness matrix.

3.1. MIXED FINITE-ELEMENT DISCRETIZATION

It is known that when standard low-order finite elements are employed to solve the Reissner-Mindlin plate, the solution degenerates very rapidly for small thickness. The use of higher-order elements (quadratic and cubic) usually avoids these difficulties, particularly when based on a mixed formulation. Following this remark, several schemes have been introduced and we refer for instance to [21, 27, 31]. In this work we deal with a quadrilateral 15-node mixed

interpolated element, here called M15. The internal variables of this model are the normal displacement and the two components of the rotation along the x and y co-ordinate axes. As to the shape functions, the finite element can be described in the following way. For each field, there are four nodal shape functions at each vertex, two side functions related to each side and three internal shape functions vanishing along the entire boundary of the quadrilateral, *i.e.*, three bubble functions. In other words, the M15 element has been obtained adding a suitable number of bubble functions to the classical serendipity space of degree three. More precisely, let $\mathcal{S}_3$ be the polynomial space of the serendipity shape functions of degree three and let $\mathcal{B}_3$ be the new space. To obtain $\mathcal{B}_3$ we take all monomials of the space $\mathcal{S}_3$ and we add the following monomial terms

$$\{x^2y^2, x^3y^2, x^2y^3\}. \tag{29}$$

A systematic analysis of this bubble plus element has been performed in previous works [33–35] which deal with the numerical solution of the Reissner-Mindlin elastic plate. Numerical experiences have evidenced that the addition of bubble functions improves the quality of the results. To overcome the locking phenomenon, non-standard formulations of the Mindlin problem are usually suggested. In this framework, some special mixed interpolated finite elements have been introduced in past years, together with a mathematical analysis proving the stability [27]. The main idea is to reduce the influence of the shear term, the contribute in the energy that generates locking, by introducing a linear operator that locally modifies the structure of the discrete space for the approximation of rotations. We will adopt such a non-standard formulation to solve the Reissner-Mindlin plate problem combined with the improved M15 finite element. In order to recall the mixed interpolated approach we consider the discretized problem corresponding to (11)

$$\begin{cases} \text{Find } (\vec{\theta}_h, w_h) \in \vec{\Theta}_h \times W_h \quad \text{such that} \\ A(\vec{\theta}_h, \eta_h) + \vec{\lambda}t^{-2}(\nabla w_h - \vec{\theta}_h, \nabla v_h - \vec{\eta}_h) = (q, v_h) \\ \forall \vec{\eta}_h \in \vec{\Theta}_h, \forall v_h \in W_h \end{cases} \tag{30}$$

where $\vec{\Theta}_h \subset (H_0^1)^2$ and $W_h \subset H_0^1$. Besides $\vec{\Theta}_h$ and W_h, a third finite-dimensional space Γ_h is needed along with a linear operator $\mathcal{R} : \vec{\Theta}_h \to \Gamma_h$. The shear energy term appearing in (30) is computed as

$$(\mathcal{R}(\nabla w_h - \vec{\theta}_h), \mathcal{R}(\nabla v_h - \vec{\eta}_h)), \tag{31}$$

instead of

$$(\nabla w_h - \vec{\theta}_h, \nabla v_h - \vec{\eta}_h). \tag{32}$$

For the sake of simplicity, it is assumed that $\mathcal{R}\nabla w_h = \nabla w_h, \forall w_h \in W_h$. The approximate problem takes then the final form

$$\begin{cases} \text{Find } (\vec{\theta}_h, w_h) \in \vec{\Theta}_h \times W_h \quad \text{such that} \\ A(\vec{\theta}_h, \eta_h) + \vec{\lambda}t^{-2}(\nabla w_h - \mathcal{R}\vec{\theta}_h, \nabla v_h - \mathcal{R}\vec{\eta}_h) = (q, v_h) \\ \forall \vec{\eta}_h \in \vec{\Theta}_h, \forall v_h \in W_h \end{cases} \tag{33}$$
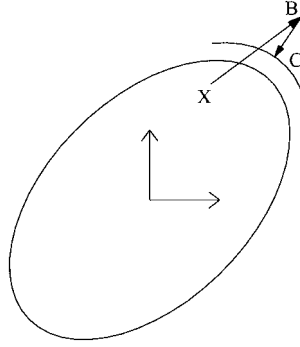
Figure 1. The return-mapping algorithm

The finite-element discretization of problem (33) calls for the choice of suitable finite element spaces, *i.e.*, $\vec{\Theta}_h$ for the approximate rotations, W_h for the approximate normal displacement and Γ_h for the approximate shear stresses. Furthermore, a linear operator $\mathcal{R}$ acting from $\vec{\Theta}_h$ to Γ_h must be chosen. We now introduce the spaces adopted in our investigation. Let $\mathcal{P}_3$ be the standard space of polynomials of degree less than or equal to three in the two variables x and y and let us define the following auxiliary space

$$\Delta_3 = \left\{ \delta = (\delta_1, \delta_2) : \delta_1 \in \mathbf{P}_3 \backslash \{x^3\}, \delta_2 \in \mathbf{P}_3 \backslash \{y^3\} \right\}, \tag{34}$$

i.e.,

$$\Delta_3 = \{ \delta = (\delta_1, \delta_2) :$$

$$\left. \begin{array}{l} \delta_1 = a_1 + \cdots + e_1 y^2 + f_1 x^2 + g_1 x^2 y + h_1 x y^2 + i_1 y^3 \\ \delta_2 = a_2 + \cdots + e_2 x^2 + f_2 y^2 + g_2 x^2 y + h_2 x y^2 + i_2 x^3 \end{array} \right\}. \tag{35}$$

Assume now that Ω is a rectangular domain, with boundary $\partial\Omega$ and let $\mathcal{T}_h$ be a decomposition of Ω in rectangles K such that $\Omega = \cup_{\mathcal{K} \in \mathcal{T}_h} K$. We define

$$\begin{aligned} \vec{\Theta}_h &= \{ \vec{\eta}_h \in \mathrm{H}_0^1(\Omega) \times \mathrm{H}_0^1(\Omega) : \vec{\eta}_h|_K \in (\mathbf{S}_3)^2 \forall K \in \mathcal{T}_h \}, \\ W_h &= \{ w_h \in \mathrm{H}_0^1(\Omega) : w_h|_K \in \mathbf{S}_3 \forall K \in \mathcal{T}_h \}, \\ \Gamma_h &= \{ \delta : \delta|_K \in \Delta_3, \delta \cdot \vec{\tau} \text{ continuous at the inter-element boundaries,} \\ &\qquad \delta \cdot \vec{\tau} = 0 \text{ on } \partial\Omega \}. \end{aligned} \tag{36}$$

Finally, a linear operator $\mathcal{R} : \vec{\Theta}_h \to \Gamma_h \subset \Delta_3$ is introduced as the one uniquely determined by the following $18 = 9 \times 2$ conditions:

$$\begin{cases} \displaystyle\int_e (\mathcal{R}(\vec{\theta}_h) - \vec{\theta}_h) \cdot \vec{\tau} p(s) \mathrm{d}s = 0 & \forall \text{ edge of } K \in \mathcal{T}_h \quad \forall p \in \mathbf{P}_2(e) \\ \displaystyle\int_K (\mathcal{R}(\vec{\theta}_h) - \vec{\theta}_h) \cdot \vec{p}(x, y) \mathrm{d}x \mathrm{d}y = 0 & \forall \vec{p} \in (\mathbf{P}_1(K))^2 \end{cases} \tag{37}$$

3.2. THE PREDICTOR-CORRECTOR ALGORITHM

The solution is supposed to be given at time t, *i.e.*, the set of variables

$$\{\Sigma_t, \mathbf{E}_t, \mathbf{E}_t^p, \overline{E}_t^p\} \tag{38}$$

is known and an update to time $t + \mathrm{d}t$ is searched for. We note that $\overline{E}^p$ is an accumulative measure of the plastic strain that is given the expression

$$\overline{E}^p = ||\mathbf{E}^p||_M, \tag{39}$$

where M is a suitable scaling matrix that relates the components of $\mathbf{E}^p$. If the solution does not violate the condition $f < 0$, *i.e.*, in the elastic case, then it represents the new solution, if not a correction has to be performed and a suitable scheme is needed to return the stress to the yield surface. To this end we resort to the classical *backward- Euler* procedure. With reference to Figure 1, starting from the (elastic) stress X, the trial stress B is mapped back to C onto the yield surface. In formulae, the backward-Euler return algorithm is based on the relationship

$$\Sigma_C = \Sigma_B - \delta\lambda\mathbf{D}\frac{\partial f}{\partial\Sigma}\bigg|_C, \tag{40}$$

where B is the elastic trial point and C is its projection onto the yield surface. An initial estimate for Σ_C may be written as

$$\Sigma_C = \Sigma_B - \delta\lambda\mathbf{D}\frac{\partial f}{\partial\Sigma}\bigg|_B, \tag{41}$$

but generally the normal at trial position B will not coincide with the final normal. In order to derive an iterative scheme to solve Equation (40), a residual vector $\mathbf{R}$ is computed that represents the difference between current stresses and backward-Euler stresses, *i.e.*,

$$\mathbf{R} = \Sigma - \left(\Sigma_B - \delta\lambda\mathbf{D}\frac{\partial f}{\partial\Sigma}|_C\right). \tag{42}$$

An iterative scheme is then set forth to reduce $||\mathbf{R}||$ to within a given tolerance. The iterative problem can be eventually cast in the form

$$\mathbf{R} = \Sigma^{n+1} - \left(\Sigma^n - \delta\lambda\frac{\partial f}{\partial\Sigma^n}\right) = 0, \tag{43}$$

$$f(\Sigma^{n+1}, \lambda) = 0, \tag{44}$$

where n is the iteration index.

4. Numerical examples

To validate the capabilities of the proposed M15 plate element in the elastoplastic regime, a variety of situations have been tested. We have considered a unit square plate with uniform decomposition in quadrilateral elements. Due to the symmetry of the domain, computations have been performed on the top-right quarter of plate only. The physical data are the following: Young's modulus $E = 10{\cdot}92$, Poisson ratio $\nu = 0{\cdot}3$, shear corrector factor $k = \frac{5}{6}$ and plate thickness $t = 10^{-1} \div 10^{-2}$. The hardening modulus H is chosen equal to zero to model an elastic perfectly plastic plate and simply supported and clamped plates are considered. Since the degrees-of-freedom of the discrete problem (30) are the rotations and the displacement, the quantities representing the stresses are obtained by a post-processing computation. The
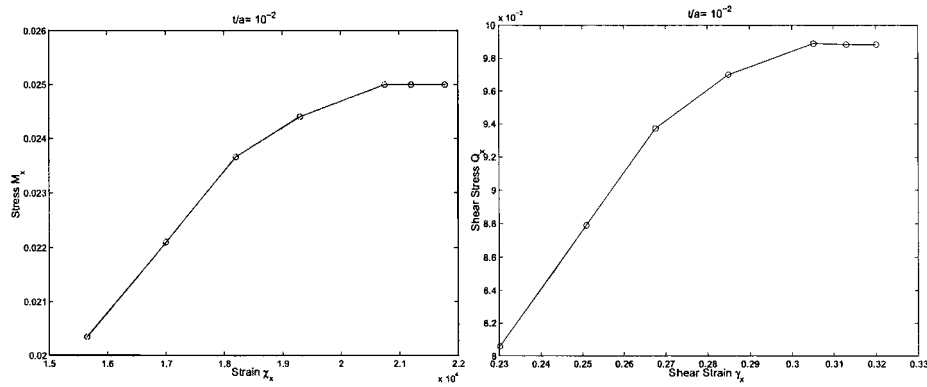
Figure 2. Simply supported plate under uniform loading $-t/a = 1/100-$ (χ_x, M_x) (left) and (γ_x, Q_x) (right) at the plate center
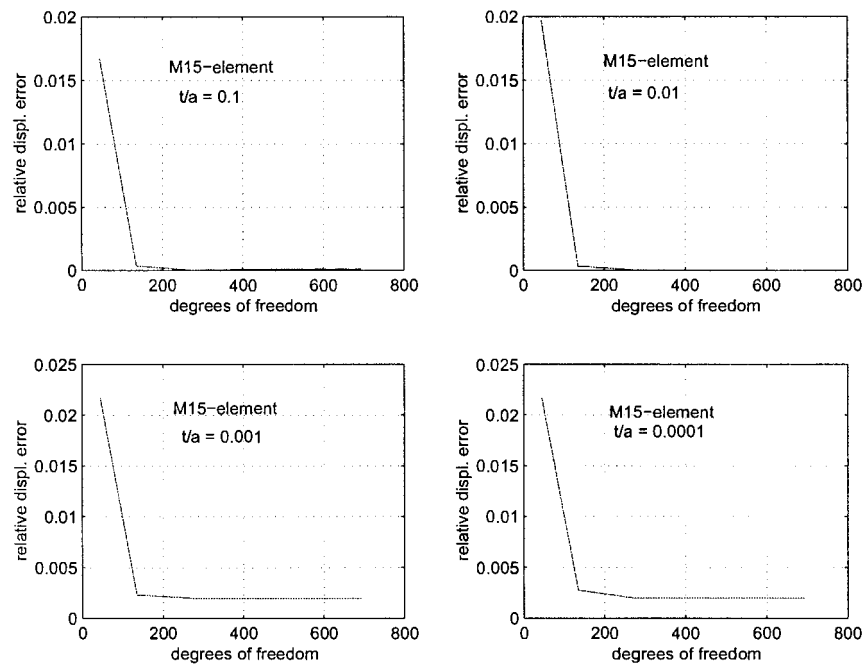

Figure 3. Relative displacement error against degrees of freedom. Clamped plate under uniform loading.

Newton-Raphson method with automatic load increase is employed to solve the nonlinear system. We note that the numerical robustness of the elasto-plastic procedure also depend on the initial elastic steps. Therefore, it is crucial to establish the reliability of the finite element employed within the elastic framework. This is shown in Figures 3 and 4, where for a range of t/a varying from 0.1 (thick plate) to 0.0001 (very thin plate), the locking was strongly reduced. The resulting element (M15) exhibits both properties of convergence and robustness as shown in [34, 35]. Furthermore, the results have been obtained on a clamped plate (see Figure 3) that is the more effective test to check the robustness of finite elements with respect to the locking effect. All computations are performed using the programming environment MODULEF [36, 37]. The numerical examples here presented are organized as follows:

1. simply supported square plate subjected to a uniform load,
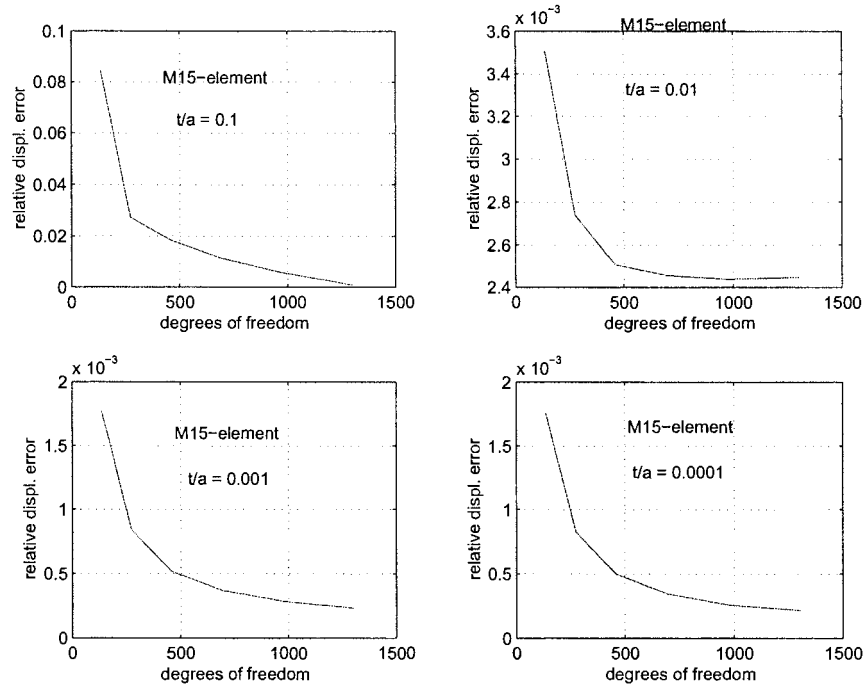
Figure 4. Relative displacement error against degrees of freedom. Simply supported plate under point load.
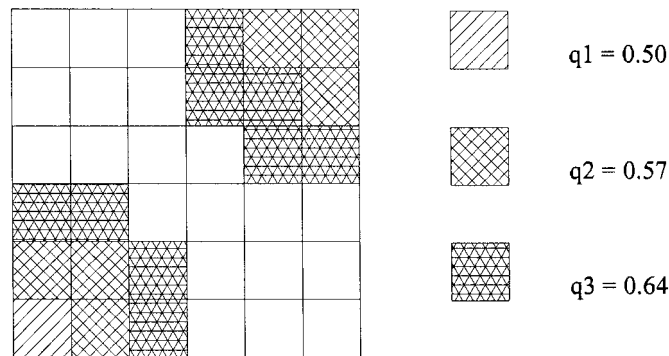

Figure 5. Top-right quarter of a simply supported plate under uniform load. Plastic zones spreading.

2. clamped square plate subjected to a uniform load,
3. simply supported square plate subjected to point load.

For each test, among others, the displacement at the centre C of the plate has been computed. Let $w_{\text{ex}}(C)$ denote the exact displacement at the centre of the plate and $w_h(C)$ the finite-element solution. The relative displacement error is defined as:

$$\frac{w_{\text{ex}}(C) - w_h(C)}{w_{\text{ex}}(C)} \times 100. \tag{45}$$

Figures 3 and 4 give the displacement error against the number of degrees of freedom for a clamped elastic plate uniformly loaded and for a simply supported plate under a point load, respectively.
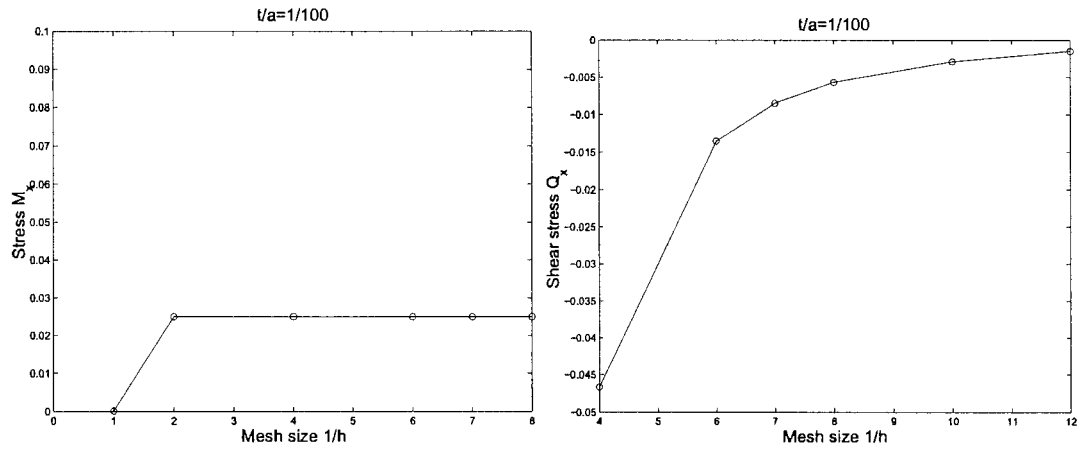
Figure 6. Simply supported plate under uniform $-t/a = 1/100-$ Plate center stresses versus mesh size reciprocal.
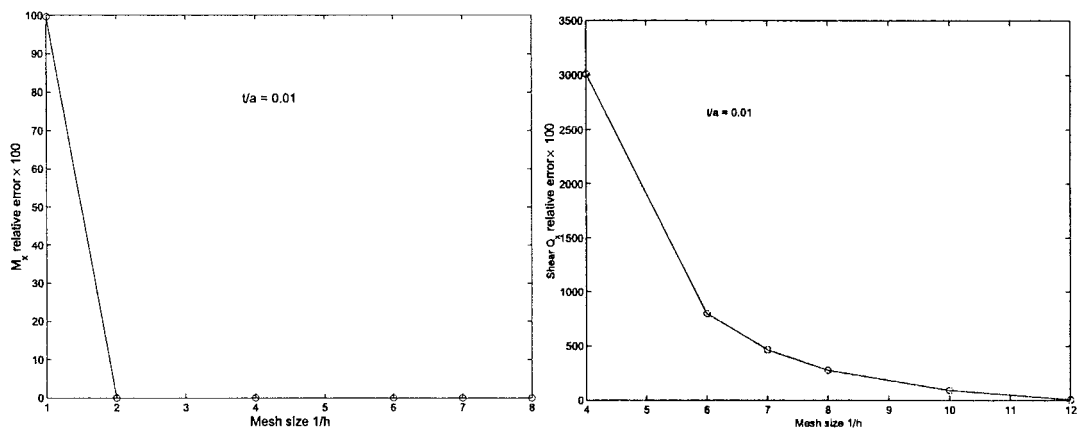

Figure 7. Simply supported plate under uniform loading $-t/a = 1/100-$ Relative stress error against degrees of freedom.
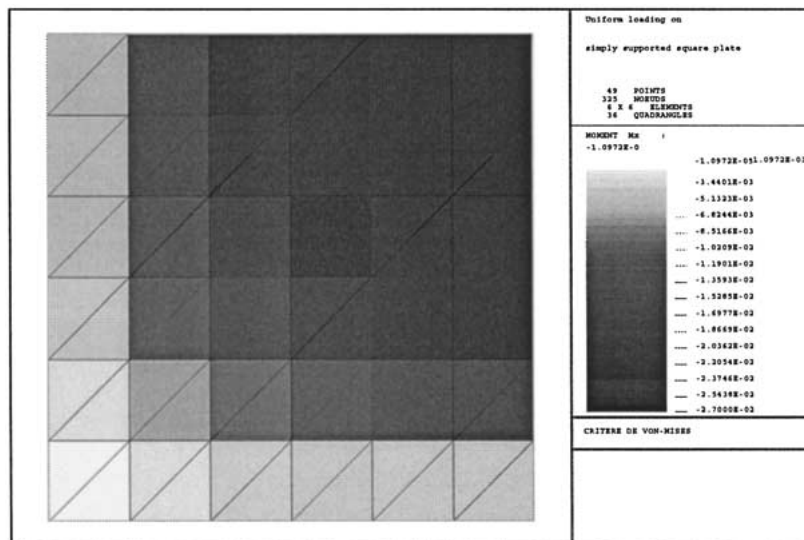

Figure 8. Top-right quarter of a simply supported plate under uniform load. Isovalues of M_X at limit load.
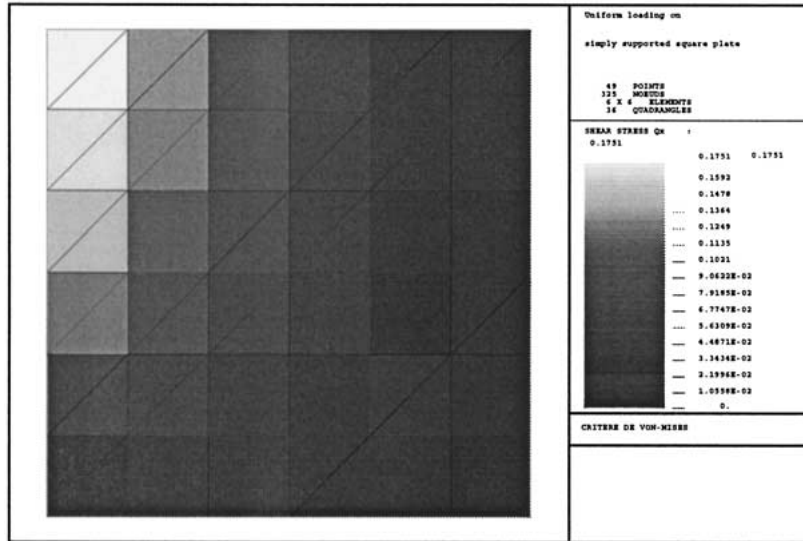
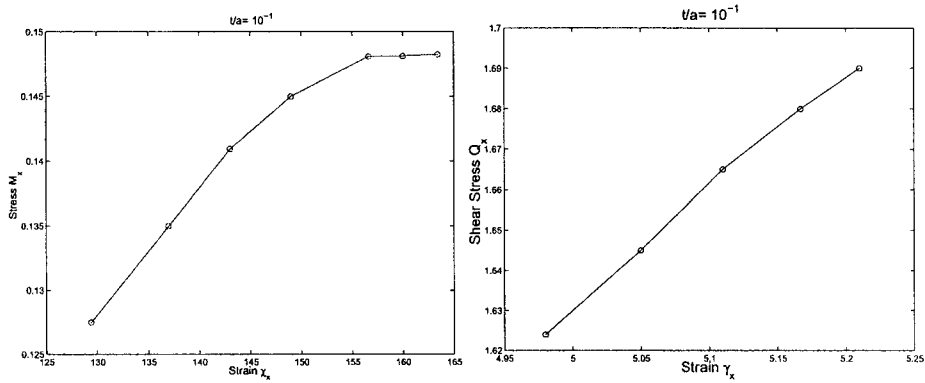*Figure 9.* Top-right quarter of a simply supported plate under uniform load. Isovalues of Q_x at limit load.

Figure 10. Clamped plate under uniform load $-t/a = 1/10 - (\chi_x, M_x)$ (left), (γ_x, Q_x) (right) at the top half corner.
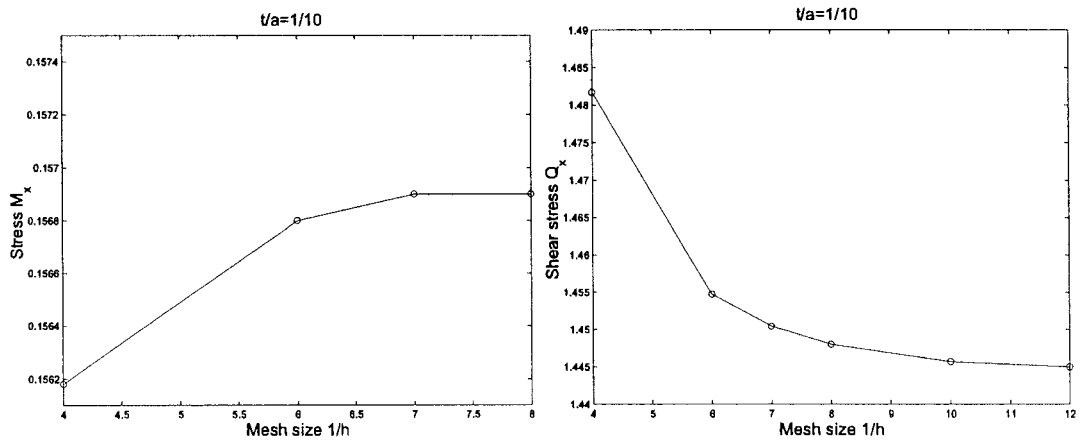

Figure 11. Clamped plate under uniform load $-t/a = 1/10-$ Top half corner stresses versus mesh size reciprocal.
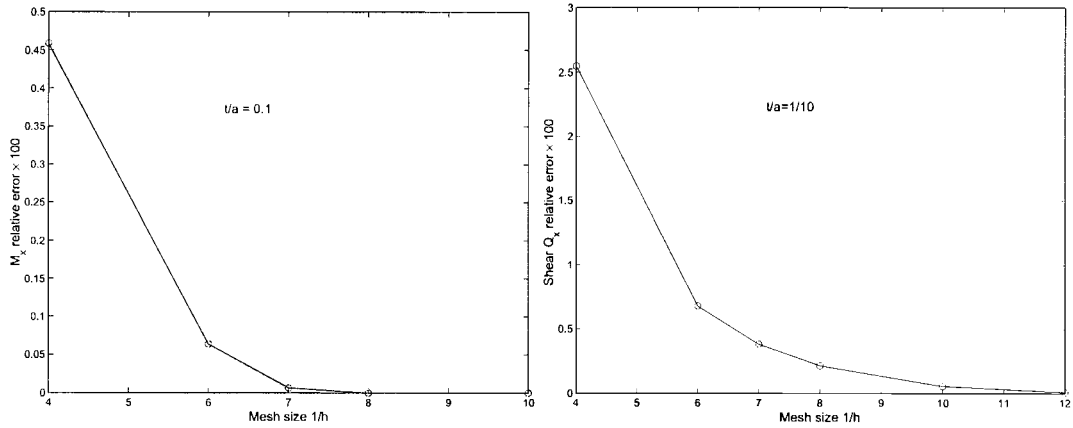
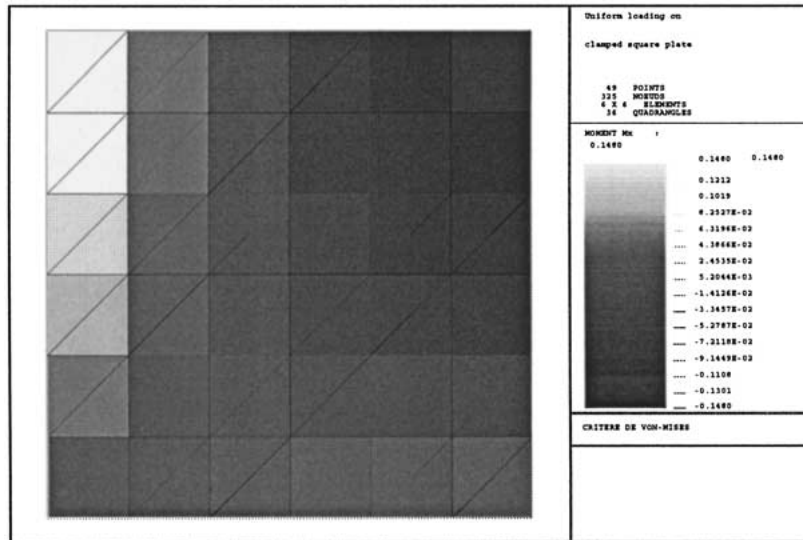*Figure 12.* Clamped plate under uniform load $-t/a = 1/10-$ Relative stress error against degrees of freedom.

Figure 13. Top-right quarter of a clamped plate under uniform load. Isovalues of M_x at limit load.

4.1. SIMPLY SUPPORTED PLATE: UNIFORM LOAD

We analyze the same square plate considered in [24] and the obtained results are compared with those presented therein. The side length is $a = 1$, the thickness $t/a = 10^{-2}$ and the initial yielding stress is $\sigma_y = 1000$. In Figure 2 we present the stress-strain diagram of type (26) obtained in this analysis; in particular, we show the variation of M_x and Q_x at the center of the plate *vs.* χ_x and γ_x, respectively. The test has been performed using a 6×6 mesh and an initial load $q_0 = 0.08$. The behavior of the plate remains elastic until a load value $q = 0.5$ is reached and the asymptotic behavior is achieved for a load $q = 0.64$. The results are in good agreement with those find in [24], where, however, a 16×16 mesh is employed. Figure 5 represents the spreading of plasticity as a function of the load level. Convergence order with respect to mesh size may be evaluated by looking at Figures 6 and 7 that shows a good trend for moments and shears as well. Shear convergence is actually known to be a delicate issue that is frequently omitted in the literature and represents a key point in favor of
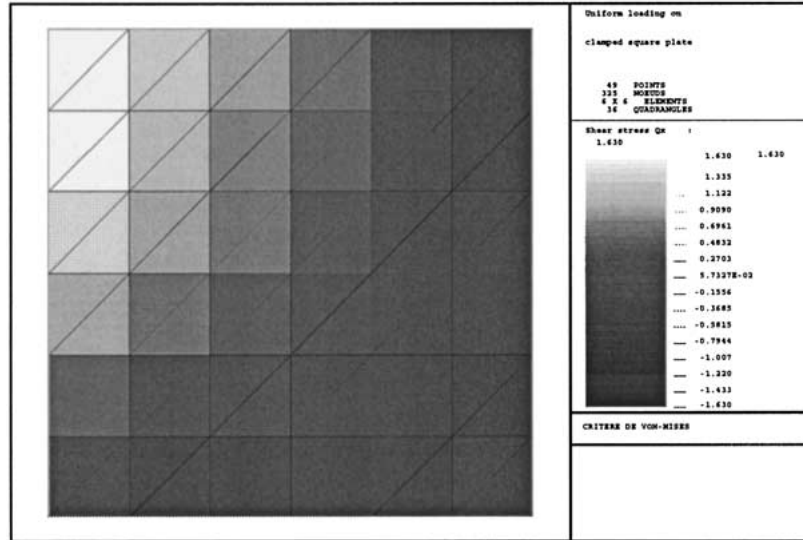
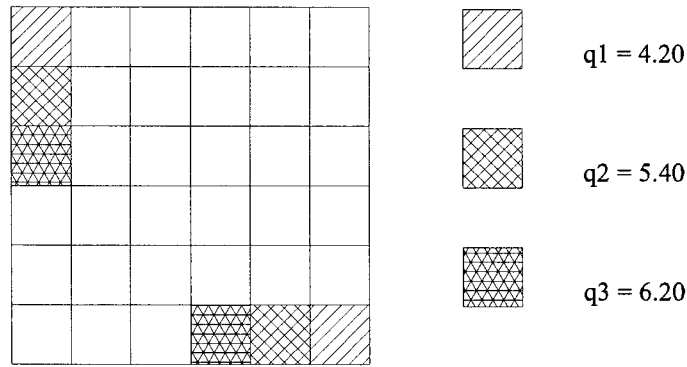*Figure 14.* Top-right quarter of a clamped plate under uniform load. Isovalues of Q_x at limit load.

Figure 15. Top-right quarter of a clamped plate under uniform load. Plastic zones spreading.

our approach. In a domain represented by the plate itself, Figures 8 and 9 show the principal stress amplitudes and the variations of M_x and Q_x.

4.2. CLAMPED PLATE UNDER UNIFORM LOAD

The clamped plate analyzed here is also tested in [23] to which we refer for comparisons. The side length is $a = 1$, the thickness $t/a = 10^{-1}$ and the yield parameter is $\sigma_y = 60$. A 6×6 mesh is used. The plate remains elastic until a load value of $q = 4.2$ is reached and attains the limit behavior for a load $q = 6.2$. With reference to the top-half corner of the plate, in Figure 10 we plot M_x *vs.* χ_x on the left and Q_x *vs.* γ_x on the right. We note that, when the moment M_x becomes plastic, the shear Q_x is still elastic. Again to assess convergence order, in Figure 11 the variation of M_x and Q_x with respect to the (reciprocal of the) mesh size is shown. Furthermore, in Figure 12 the relative stress error against degrees of freedom is shown. The distribution of the principal stresses M_x, and Q_x are given in Figures 13 and 14, respectively. The evolution of plastic strain within the plate may be appreciated by looking at Figure 15.
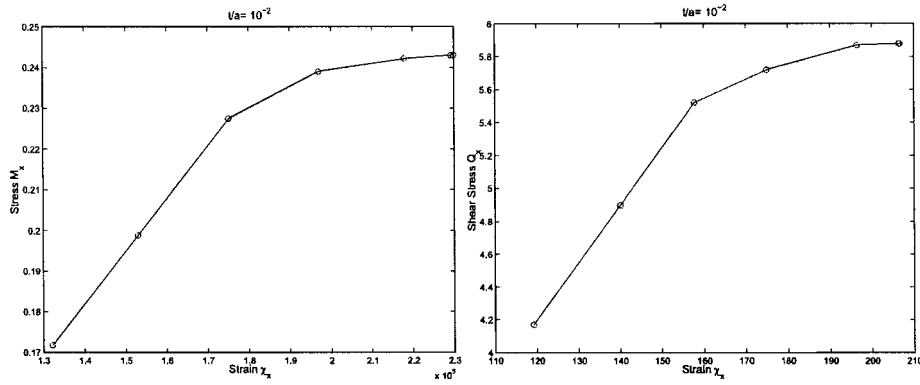
Figure 16. Simply supported plate under point load $-t/a = 1/100 - (\chi_x, M_x)$ (left), (γ_x, Q_x) (right) at the plate center.
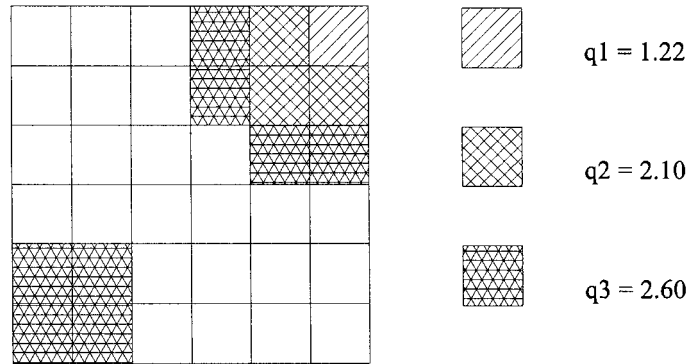

Figure 17. Top-right quarter of a simply supported plate under point load. Plastic zones spreading.

4.3. POINT LOAD ON SIMPLY SUPPORTED PLATE

As a last test problem we take a simply supported square plate loaded by a point load in the center. The side length is $a = 1$, the thickness $t/a = 10^{-2}$ and the yield parameter is $\sigma_y = 1000$, namely the same plate considered in [24]. During the elastic response the presented finite element is very effective. With reference to [44], using a new set of suitable bubble functions (Equation 29) the M15 element becomes able to capture the singularity and for a unit point load the elastic discrete solution converges to the analytical solution of [43]. Further increasing the load leads to plastic deformations that occur once the load reaches the critical value $q = 1 \cdot 22$. As in previous examples, Figure 16 shows the stress-strain curves (M_x, χ_x) and (Q_x, γ_x). The spreading of plastic strains is given in Figure 17 where point load values of $q = 1 \cdot 46$ and $q = 2 \cdot 6$ are shown to be the initial and limit loads.

5. Conclusions and future work

Peculiar delicate issues associated to the modelling and numerical analysis of elastoplastic plates were tackled in this paper. The Reissner-Mindlin idealization was considered to start with but attention was paid also to the thin limit, *i.e.*, to the Kirchhoff model.

Moving from the elastic theory that is nowadays well understood and for which several FEM-based discretization schemes are available, a viable variational formulation of the

elastic-plastic problem was proposed as a fundamental step toward the development of our numerical approach. An elastic-predictor plastic-corrector type of algorithm was proposed that operates directly on structural static and kinematic quantities (moments, shears, curvatures and rotations), rather than on classical stress and strain tensors of continuum mechanics. Standard J_2 Mises plasticity was assumed as to the yield function and an iterative backward Euler scheme represents the core of the proposed return-mapping approach.

Hierarchical finite elements were introduced for the discretization of the continuous problems that were devised and numerically tested in the recent past in the elastic regime. Stable approximations to the continuous problems were obtained thanks to the adoption of serendipity plus bubble elements. The procedure was shown to be free of locking all the way through the very thin limit. The adopted discretization was shown to be able to handle the singular behavior associated to point normal loads.

Different boundary conditions and external loads were considered and convergence with respect to the mesh size assessed either for usual entities such as centroidal deflection and bending moments and for more critical quantities such as shears. Among the few results available in the literature for the sake of comparison, those reported in [23] and [24] were considered and an excellent agreement between our approach and the one proposed therein was found.

Among the undergoing extensions, applications of the proposed numerical scheme to the case of functionally graded plates, at least in the elastic regime, are worth mentioning in view of the wide variety of design possibilities that such new types of material offer to the practitioner.

References

1. T.J.R. Hughes and J.R. Stewart, A space-time formulation for multiscale phenomena. *J. Comp. Appl. Math.* 74 (1996) 217–229.
2. A. Carpinteri and B. Chiaia, Multifractal scaling laws in the breaking behaviour of disordered materials. *Chaos, Solitons and Fractals* 8 (1997) 135–150.
3. I. Carol and K. Willam, Spurious energy dissipation/generation in stiffness recovery models for elastic degradation and damage. *Int. J. Solids Structs.* 33 (1996) 2939–2957.
4. B. Loret and E. Rizzi, Strain localization in fluid-saturated anisotropic elastic-plastic porous media. *Int. J. Eng. Sci.* 37 (1999) 235–251.
5. Z.P. Bazant, Size Effect Aspects of Measurement of Fracture Characteristics of Quasibrittle Material. *Adv. Cement Based Materials* 4(3–4) (1996) 128–137.
6. M.G.D. Geers, R. de Borst and R.H.J. Peerlingsa, Damage and crack modeling in single-edge and double-edge notched concrete beams. *Eng. Fract. Mech.* 65 (2000) 247–261.
7. M.E. Gurtin, *Configurational Forces as Basic Concepts of Continuum Physics.* New York: Springer-Verlag (2000) 249 pp.
8. P.M. Mariano and F.L. Stazi, Strain localization in elastic micro-cracked bodies, *Comp. Meth. Appl. Mech. Eng.* 190 (2001) 5657–5677.
9. J. Lubliner, *Plasticity Theory.* New York: Macmillan (1990) 495 pp.
10. J.C. Simo and T.J.R. Hughes, *Computational Inelasticity.* New York: Springer-Verlag (1997) 392 pp.
11. T. Belytschko, W.K. Liu and B. Moran, *Nonlinear Finite Elements for Continua and Structures.* Chichester: Wiley (2000) 650 pp.
12. M.A. Crisfield, *Non-Linear Finite Element Analysis of Solids and Structures, vol. 1-2.* Swansea: Wiley (1991) 271 pp.
13. D.R.J. Hinton and E. Hinton, *Finite Elements in Plasticity.* Swansea: Pineridge Press (1980) 594 pp.
14. T.J.R. Hughes, R.L. Taylor and W. Kanoknukulchai, A simple and efficient finite element for plate bending. *Int. J. Num. Meth. Engng.* 11 (1977) 1529–1543.

15. J.K. Batoz, K.-J. Bathe and L. Ho, A study of three-node triangle plate bending, elements. *Int. J. Num. Meth. Engng.* 15 (1980) 1771–1812.
16. R.K.N.D. Rajapakse and A.P.S. Selvadurai, On the performance of Mindlin plate elements in modelling plate-elastic medium interaction: a comparative study. *Int. J. Num. Meth. Engng.* 23 (1986) 1229–1244.
17. J.N. Reddy, *Mechanics of Laminated Composite Plates: Theory and Analysis.* Bocar Raton: CRC Press (1997) 782 pp.
18. E. Reissner, The effect of transverse shear deformation on the bending of elastic plates. *J. Appl. Mech.* 23 (1945) 69–77.
19. R.D. Mindlin, Influence of rotary inertia and shear on flexural motion of isotropic, elastic plates. *J. Appl. Mech.* 18 (1951) 31–38.
20. J.C. Simo and J.M. Kennedy, Finite strain elastoplasticity in stress resultant-geometrically exact shell. *Proc. COMPLAS II*, Barcelona (1989) 651–670.
21. K-J. and E. Dvorkin, A four-node plate bending element based on Mindlin-Reissner plate theory and mixed interpolation. *Int. J. Num. Meth. Engng.* 21 (1985) 367–383.
22. P. Papadopoulos and R.L. Taylor, An analysis of inelastic Reissner-Mindlin plates. *Finite Elements Analysis Design* 10 (1991) 221–223.
23. F. Auricchio and R.L. Taylor, A generalized elastoplastic plate theory and its algorithmic implementation. *Int. J. Num. Meth. Engng.* 37 (1994) 2583–2608.
24. A. Ibrahimbegovic and F. Frey, An efficient implementation of stress resultant plasticity in analysis of Ressner-Mindlin plates. *Int. J. Num. Meth. Engng.* 36 (1993) 303–320.
25. C.P. Providakis and D.E. Beskos, Inelastic transient dynamic analysis of Reissner-mindlin plates by the D/BEM. *Int. J. Num. Meth. Engng.* 49 (2000) 383–397.
26. K-J. Bathe, *Finite Element Procedures.* Englewood Cliffs, New Jersey: Prentice Hall (1996) 1037 pp.
27. F. Brezzi, K-J. Bathe and M. Fortin, Mixed-interpolated elements for Reissner-Mindlin plates. *Int. J. Num. Meth. Engng.* 28 (1990) 1787–1801.
28. T.J.R. Hughes, *The Finite Element Method.* Englewood Cliffs, New Jersey: Pretience-Hall (1987) 682 pp.
29. O.C. Zienkiewicz and R.L. Taylor, *The Finite Element Method.* New York: McGraw-Hill (1989) 459 pp.
30. I. Babuška: The p and $h - p$ versions of the finite element method. The state of the art. In: D.L. Dwoyer, M.Y. Hussaini, R.. Voigt (eds), *Finite elements, Theory and Application.* New York: Springer-Verlag (1988) 199–239.
31. L. DellaCroce and T. Scapolla, Hierarchic finite elements for moderately thick to very thin plates. *Comp. Mech.* 10 (1992) 263–279.
32. L. DellaCroce and T. Scapolla, Hierarchic finite elements with selective and uniform reduced integration for Reissner-Mindlin plates. *Comp. Mech.* 10 (1992) 121–131.
33. L. DellaCroce and T. Scapolla, Transverse shear strain approximation for the Reissner-Mindlin plate with high order hierarchic finite elements. *Mech. Res. Comm.* 20 (1993) 1–7.
34. L. DellaCroce and T. Scapolla, Serendipity and bubble plus hierarchic finite elements for thin and thick plates. *Struct. Eng. Mech.* 9 (2000) 433–448.
35. L. DellaCroce and T. Scapolla, Hierarchic and mixed-interpolated finite elements for Reissner-Mindlin problems. *Comm. Num. Meth. Engng.* 11 (1995) 549–562.
36. P.L. George and P. Laug, Normes d'utilisazion et de programmation MODULEF-INRIA (1982).
37. Modulef Installation page. http://www-rocq.inria.fr/modulef
38. W. Han and B.D. Reddy, *Plasticity: Mathematical Theory and Numerical Analysis.* New York: Springer (1999) 371 pp.
39. B.D. Reddy, Mixed variational inequalities arising in elastoplasticity. *Nonlin. Anal.* 19 (1992) 1071–1089.
40. B.D. Reddy, *Introductory Functional Analysis.* New York: Springer (1998) 471 pp.
41. G.S. Shapiro, On yield surfaces for ideally plastic shells. *Prob. Contin. Mech.* 10 (1961) 414–418.
42. G.V. Ivanov, Approximating the final relationship between the forces and moments of shells under the Mises plasticity condition. *Mekhanika Tverdogo Tela.* 2 (1967) 74–75.
43. S. Timoshenko and S. Woinowski-Krieger, *Theory of Plates and Shells.* New York: McGraw Hill (1970) 345 pp.
44. T. Scapolla and L. DellaCroce, Numerical solution of singularly loaded Reissner-Mindlin Plates with hierarchic serendipity and bubble plus finite elements, In: M. Feistauer, R. Rannacher and K. Kozel (eds.), *Proceedings of the 2nd Summer Conference on Numerical Modelling in Continuum Mechanics.* (1994) pp. 235–245.